SI Materials and Methods

Selection of prefusion and postfusion PIV3 F-specific human monoclonal antibodies. 171 human sera were screened for PIV3 neutralization using a GFP reporter assay and the most potent neutralizers were selected for B-cell culture. IgG+ memory B cells were isolated by cell sorting and immortalized in clonal conditions using Epstein Barr Virus and CpG as described (1). Culture supernantants were screened using recombinant proteins and PIV3 neutralization to isolate antibodies specific for the pre- and post-fusion conformation of the PIV3 F protein. Individual B-cell supernatants were assessed for neutralization potency and binding to a recombinant postfusion PIV3 F glycoprotein trimer (*SI Appendix,* Fig. S1*B*). B-cell clones showing either potent neutralization and low binding to postfusion F glycoprotein (PIA3 and PIA174) or low neutralization and high binding to postfusion F glycoprotein (PIA56 and PIA75) were sequenced and expressed as recombinant monoclonal antibodies (*SI Appendix*, Table S1).

Structure-based design of prefusion PIV3 F glycoprotein trimers. Using the homologous model from the PIV5 prefusion glycoprotein crystal structure (PDB ID 4GIP, 4WSG) we designed 29 disulfide bonds, 58 cavity-filling mutations, 12 helix-disrupting mutations, 26 combinations of disulfides and cavity-filling mutations and 6 changes in the C-terminal stem (Fig. 1*B* and *SI Appendix,* Table S1). By co-expression of the PIA3 or PIA174 Fabs with the PIV3 F glycoprotein with a C-terminal GCN4 coiled coil, we isolated antibody-F complexes which showed clear prefusion conformation for the F trimer (*SI Appendix,* Fig. S1*C,* top panels) with the PIA3 Fab binding in a 3:1 ratio (Fab:trimer) near an epitope similar to the RSV F site Ø, and the PIA174 Fab binding in a 1:1 ratio (Fab:trimer) at the apex of the trimer in a similar manner to some HIV-1 broadly neutralizing antibodies PGT145 or VRC26.09 (2, 3). Using these

PIV3 prefusion and postfusion F-specific antibodies PIA3, PIA174, PIA56 and PIA75 and an anti-Strep Tag II antibody (IBA), the designs were assessed for their ability to specifically bind the prefusion-specific antibodies versus the postfusion-specific antibodies and express at high yield (*SI Appendix*, Table S1). F constructs yielding high binding titers to prefusion specific antibodies were expressed and biophysical, structural and antigenic characteristics determined to confirm the prefusion conformation (*SI Appendix*, Fig. S1*C* lower panels, S2). Using negative stain EM as a readout for conformation, prefusion-stabilized PIV3 F glycoprotein trimers containing various disulfide-stabilizing designs displayed almost 100% retention of the prefusion conformation at 37°C in PBS for 4 weeks while the cavity-fillingstabilized PIV3 F glycoprotein showed a marked reduction of prefusion conformation during this timeframe (Fig. 1*C*).

Protein expression and purification. PIV F glycoproteins were expressed by transfection in 293F cells (Thermo Fisher) using Turbo293 transfection reagent (SPEED BioSystem) according to the manufacturer's protocol. Transfected cells were incubated in shaker incubators at 120 rpm, 37°C, 9% CO_2 overnight. On the second day, one tenth culture volume of CellBooster medium (ABI scientific) was added to each flask of transfected cells and cell cultures were incubated at 120 rpm, 37°C, 9% CO_2 for an additional 5 days. 6 days post-transfection, cell culture supernatants were harvested and proteins were purified from the supernatants using tandem Ni^{2+} (Roche) and Streptactin (IBA) affinity purification. The C-terminal purification tags were removed by thrombin digestion at room temperature overnight and proteins were further purified by SEC in a Superdex 200 column (GE) in PBS.

Antigenic screening of PIV F immunogens. Initial assessment of all constructs were performed using a 96-well microplate format for high throughput expression followed by an ELISA-based antigenic evaluation as described previously (4). Briefly, 24 h prior to transfection HEK 293T cells (Thermo Fisher Scientific, MA) were seeded in each well of a 96-well microplate at a density of $2.5x10^5$ cells/ml in expression medium (high glucose DMEM supplemented with 10% ultra-low IgG fetal bovine serum and 1x-non-essential amino acids), and incubated at 37°C, 5% CO_2 for 20 h. Plasmid DNA and TrueFect-Max (United BioSystems, MD) were mixed and added to the growing cells, and the 96-well plate incubated at 37°C, 5% CO_2. One day post transfection, enriched medium (high glucose DMEM plus 25% ultra-low IgG fetal bovine serum, 2x nonessential amino acids, 1x glutamine) was added to each well, and the 96-well plate was returned to the incubator for continuous culture. Five days post transfection, supernatants with the expressed PIV F variants were harvested and tested by ELISA for binding to PIA3, PIA174, PIA56 and PIA75 antibodies using Ni^{2+}-NTA microplates.

PIV F antigenic characterization. A fortéBio Octet Red384 instrument was used to measure binding kinetics of PIV3 F variants to antibodies that target the prefusion or postfusion F form (PIA3, PIA174, PIA56 and PIA75). All assays were performed with agitation set to 1,000 rpm in phosphate-buffered saline (PBS) supplemented with 1% bovine serum albumin (BSA) to minimize nonspecific interactions. The final volume for all solutions was 50 µl/well. Assays were performed at 30°C in tilted black 384-well plates (Geiger Bio-One). Ni-NTA sensor tips were used to capture relevant PIV F variants. Typical capture levels for each loading step were between 1.4 and 1.5 nm, and variability within a row of eight tips did not exceed 0.1 nm for each of these steps. Biosensor tips were equilibrated for 120 s in PBS + 1% BSA prior to loading PIV

F variants. Biosensor tips were then equilibrated for 120 s in PBS + 1% BSA prior to measuring association with antigen binding fragments (Fabs) in solution (0.007 μM to 1.0 μM) for 300 s; Fabs were then allowed to dissociate for 300-1,200 s depending on the observed dissociation rate. Parallel correction to subtract systematic baseline drift was carried out by subtracting the measurements recorded for a loaded sensor incubated in PBS + 1% BSA. Data analysis and curve fitting were carried out using Octet software, version 9.0. Experimental data were fitted with the binding equations describing a 1:1 interaction. Global analysis of the data sets assuming reversible binding (full dissociation) were carried out using nonlinear least-squares fitting allowing a single set of binding parameters to be obtained simultaneously for all of the concentrations used in each experiment.

Physical stability of RSV F variants. To assess the physical stability of the prefusion conformation of designed PIV F glycoproteins under various stress conditions, we treated the proteins with a variety of pharmaceutically relevant stresses such as extreme pH, high temperature, low and high osmolarity, and repeated freeze/thaw cycles while at a concentration of 50 μg/ml. The physical stability of treated PIV F variants was evaluated by the preservation of binding to prefusion-specific antibodies PIA3 and PIA174. In pH treatments, the PIV F glycoprotein solution was adjusted to pH 3.5 and pH 10 with appropriate buffers and incubated at room temperature for 60 minutes and subsequently neutralized to pH 7.5. Temperature treatments were carried out by incubating the PIV F glycoprotein solutions at 50°C and 70°C for 60 minutes in a PCR cycler with heated lid. In osmolarity treatments, PIV F glycoprotein solutions originally containing 150 mM NaCl were either diluted with 2.5 mM Tris buffer (pH 7.5) to an osmolarity of 10 mM NaCl or adjusted with 4.5 M $MgCl_2$ to a final concentration of

3.0 M $MgCl_2$. Protein solutions were incubated for 60 minutes at room temperature and then returned to 150 mM salt by adding 5.0 M NaCl or dilution with 2.5 mM Tris buffer, respectively, and concentrated to 50 μg/ml. The freeze/thaw treatment was carried out by repeatedly freezing PIV F glycoprotein solutions in liquid nitrogen and thawing at 37°C ten times in the presence of 10% glycerol. All PIV F glycoproteins were diluted to 40 μg/ml with PBS + 1% BSA, and their ability to bind PIA3 and PIA174 Fab was measured with an Octet instrument using the protocol described above. The degree of physical stability is reported as the ratio of steady state prefusion antibody-binding level before and after stress treatment.

Negative-stain electron microscopy. Proteins were diluted with 10 mM HEPES, pH 7.0, 150 mM NaCl, adsorbed to a freshly glow-discharged carbon-film grid, washed with the same buffer, and stained with 0.7% uranyl formate. Images were collected at a magnification of 100,000 using SerialEM (5) on an FEI Tecnai T20 microscope equipped with a 2k x 2k Eagle CCD camera and operated at 200 kV. The pixel size was 0.22 nm. Particles were picked using the swarm mode in e2boxer from the EMAN2 software package (6), followed by manual corrections. Reference-free 2D classifications were performed using EMAN2 and SPIDER (7). To determine fractions of prefusion and postfusion molecules, each particle in a dataset was aligned automatically using SPIDER to either a selection of 2D class averages (PIV1, 2, 4) or projections of negative-stain 3D maps (PIV3) representing the two conformations. Each particle was then assigned to either the prefusion or postfusion fraction based on the highest value of cross-correlation coefficient.

Cryo-EM data collection and processing. The PIV3 Q162C-L168C, I213C-G230C, A463V, I474Y Env at a final concentration of 0.5 mg/mL was incubated with 3–fold molar excess of the

PIA174 Fab fragments for 2 hours. To prevent aggregation during vitrification, the sample was incubated in 0.085 mM dn-Dodecyl β-D-maltoside (DDM), followed by vitrification using a semi-automated Spotiton V1.0 robot (8, 9). The grids used were nanowire self-blotting grids with a lacey carbon support substrate (10). Sample was dispensed onto the nanowire grids using a picoliter piezo dispensing head. A total of ~5 nL sample, dispensed as 50 pL droplets, was applied in a stripe across each grid, followed by a pause of a few milliseconds, before the grid was plunged into liquid ethane.

Data were acquired using the Leginon system (11) installed on a Titan Krios electron microscope operating at 300kV, fitted with a Gatan K2 Summit direct detection device and an energy filter. The dose was fractionated over 50 raw frames and collected over a 10-s exposure time. Individual frames were aligned and dose-weighted (12). CTF was estimated using the GCTF package (13). Particles were picked using DoG Picker (14) within the Appion pipeline (15). Particles were extracted from the micrographs using RELION (16). 2D classification, *ab initio* reconstruction, heterogeneous refinement, and final map refinement were performed using cryoSparc (17). Postprocessing was performed within RELION.

Model fitting. For fitting into the cryo-EM reconstructions we constructed homologous models of the PIV3 Env trimer and PIA174 Fab from the PIV5 prefusion glycoprotein crystal structures (PDB ID 4GIP, 4WSG) and VRC01 coordinates (PDB ID 4LSS), respectively, using SWISS-MODEL (18). Fits of the PIV3 trimer and Fab coordinates to the cryo-EM reconstructed maps were performed using UCSF Chimera (19). The coordinates were refined by an iterative process of manual fitting using Coot (20) and real space refinement within Phenix (21). Molprobity (22) and EMRinger (23) were used to check geometry and evaluate structures at each iteration step.

Figures were generated in UCSF Chimera and Pymol (www.pymol.org). Map-fitting cross correlations were calculated using Fit-in-Map feature in UCSF Chimera. Map-to-model FSC curves were generated using EMAN2 (6).

Immunogenic characterization of PIV F glycoprotein trimer designs in mice

To assess the effectiveness of recombinant PIV3 prefusion F trimer designs at eliciting neutralizing antibodies, groups of 10 CB6F1/J mice were immunized twice at weeks 0 and 3 intramuscularly with 10 μg of recombinant PIV3 F glycoprotein trimer designs combined with 10 μg Poly I:C and week 5 sera assessed for heterologous PIV3 virus neutralization *in vitro*. For PIV1, 2 and 4 F immunizations, groups of 10 CB6F1/J mice were immunized twice at weeks 0 and 3 with 10 μg of recombinant PIV F glycoprotein trimer designs combined with 10 μg Poly I:C and week 5 sera assessed for heterologous PIV neutralization *in vitro.* Similarly for the quadrivalent and trivalent immunization in mice the same immunization protocol was performed, with serum neutralization redout using PIV1, 2, 3 or 4 viruses. Neutralizing antibody titers were determined using a microneutralization assay using GFP-expressing PIV1 (Washington/20993/1964), PIV2 (V94(15C), or PIV3 (JS strain) viruses (ViraTree) and LLC-MK2 cells. Culture supernatants or serum dilutions were incubated for 1 h at room temperature with an appropriate concentration of PIV1, PIV2, or PIV3 viruses, leading to approximately 80% GFP^+ cells before addition of LLC-MK2 cells. The cultures were analyzed using a BD Pathway bioimaging system on day 3 post infection for PIV3 and on day 5 and 7 for PIV2 and PIV1, respectively. The 50% inhibitory dilution (ID_{50}) was determined. In the case of PIV4 strain, microneutralization assay was performed using PIV4a (M-25 strain, ATCC VR-1378) and H292 cells. Sera dilutions were incubated for 1 hr at 37 °C with PIV4a leading to 80% cells infection

and later H292 cells were added. On the day after, the virus input was washed out and complete medium containing 45 μg/ml TPCK treated trypsin (Worthington Biochemical LS003750) was added and the cells incubated for additional 5 days. The culture were permeabilized and stained with Light Diagnostics™ Parainfluenza 4 Antibody FITC Reagent (Millipore 5034) and DraQ5 (Thermos Scientific 62251) and read with a Mirrorbal fluorescence cytometer (TTP Labtech).

Immunogenic characterization of PIV F glycoprotein trimer designs in non-human primates. All animal experiments were reviewed and approved by the Animal Care and Use Committee of the Vaccine Research Center, NIAID, NIH and all animals were housed and cared for in accordance with local, state, federal and institute policies in an American Association for Accreditation of Laboratory Animal Care (AAALAC)-accredited facility at the NIH. Female and male Indian rhesus macaques with body weights between 2-9 kg were used for immunization studies. For each immunization, 1 ml of immunogen mix, containing 100 μg of the specified, filter-sterilized protein immunogen and 500 μl of poly(IC:LC) (Oncovir, DC) (24, 25) in PBS, was injected via a needle syringe into the caudal thighs of the two hind legs. Blood was collected two weeks post immunization for serological analyses.

REFERENCES

1. Traggiai E, *et al.* (2004) An efficient method to make human monoclonal antibodies from memory B cells: potent neutralization of SARS coronavirus. *Nat Med* 10(8):871-875.
2. Doria-Rose NA, *et al.* (2014) Developmental pathway for potent V1V2-directed HIV-neutralizing antibodies. *Nature* 509(7498):55-62.
3. Lee JH, *et al.* (2017) A Broadly Neutralizing Antibody Targets the Dynamic HIV Envelope Trimer Apex via a Long, Rigidified, and Anionic beta-Hairpin Structure. *Immunity* 46(4):690-702.
4. McLellan JS, *et al.* (2013) Structure-based design of a fusion glycoprotein vaccine for respiratory syncytial virus. *Science* 342(6158):592-598.
5. Mastronarde DN (2005) Automated electron microscope tomography using robust prediction of specimen movements. *J Struct Biol* 152(1):36-51.
6. Tang G, *et al.* (2007) EMAN2: an extensible image processing suite for electron microscopy. *J Struct Biol* 157(1):38-46.
7. Frank J, *et al.* (1996) SPIDER and WEB: processing and visualization of images in 3D electron microscopy and related fields. *J Struct Biol* 116(1):190-199.
8. Razinkov I, *et al.* (2016) A new method for vitrifying samples for cryoEM. *J Struct Biol* 195(2):190-198.
9. Dandey VP, *et al.* (2018) Spotiton: New features and applications. *J Struct Biol* 202(2):161-169.
10. Wei H, *et al.* (2018) Optimizing "self-wicking" nanowire grids. *J Struct Biol* 202(2):170-174.
11. Suloway C, *et al.* (2005) Automated molecular microscopy: the new Leginon system. *J Struct Biol* 151(1):41-60.
12. Zheng SQ, *et al.* (2017) MotionCor2: anisotropic correction of beam-induced motion for improved cryo-electron microscopy. *Nat Methods* 14(4):331-332.
13. Zhang K (2016) Gctf: Real-time CTF determination and correction. *J Struct Biol* 193(1):1-12.
14. Voss NR, Yoshioka CK, Radermacher M, Potter CS, & Carragher B (2009) DoG Picker and TiltPicker: software tools to facilitate particle selection in single particle electron microscopy. *J Struct Biol* 166(2):205-213.
15. Lander GC, *et al.* (2009) Appion: an integrated, database-driven pipeline to facilitate EM image processing. *J Struct Biol* 166(1):95-102.
16. Scheres SH (2012) RELION: implementation of a Bayesian approach to cryo-EM structure determination. *J Struct Biol* 180(3):519-530.
17. Punjani A, Rubinstein JL, Fleet DJ, & Brubaker MA (2017) cryoSPARC: algorithms for rapid unsupervised cryo-EM structure determination. *Nat Methods* 14(3):290-296.
18. Waterhouse A, *et al.* (2018) SWISS-MODEL: homology modelling of protein structures and complexes. *Nucleic Acids Res* 46(W1):W296-W303.
19. Pettersen EF, *et al.* (2004) UCSF Chimera--a visualization system for exploratory research and analysis. *J Comput Chem* 25(13):1605-1612.
20. Emsley P & Cowtan K (2004) Coot: model-building tools for molecular graphics. *Acta Crystallogr D Biol Crystallogr* 60(Pt 12 Pt 1):2126-2132.
21. Adams PD, *et al.* (2004) Recent developments in the PHENIX software for automated crystallographic structure determination. *J Synchrotron Radiat* 11(Pt 1):53-55.

22. Davis IW, Murray LW, Richardson JS, & Richardson DC (2004) MOLPROBITY: structure validation and all-atom contact analysis for nucleic acids and their complexes. *Nucleic Acids Res* 32(Web Server issue):W615-619.
23. Barad BA, *et al.* (2015) EMRinger: side chain-directed model and map validation for 3D cryo-electron microscopy. *Nat Methods* 12(10):943-946.
24. Faria NR, *et al.* (2014) HIV epidemiology. The early spread and epidemic ignition of HIV-1 in human populations. *Science* 346(6205):56-61.
25. Flynn BJ, *et al.* (2011) Immunization with HIV Gag targeted to dendritic cells followed by recombinant New York vaccinia virus induces robust T-cell immunity in nonhuman primates. *Proc Natl Acad Sci U S A* 108(17):7131-7136.

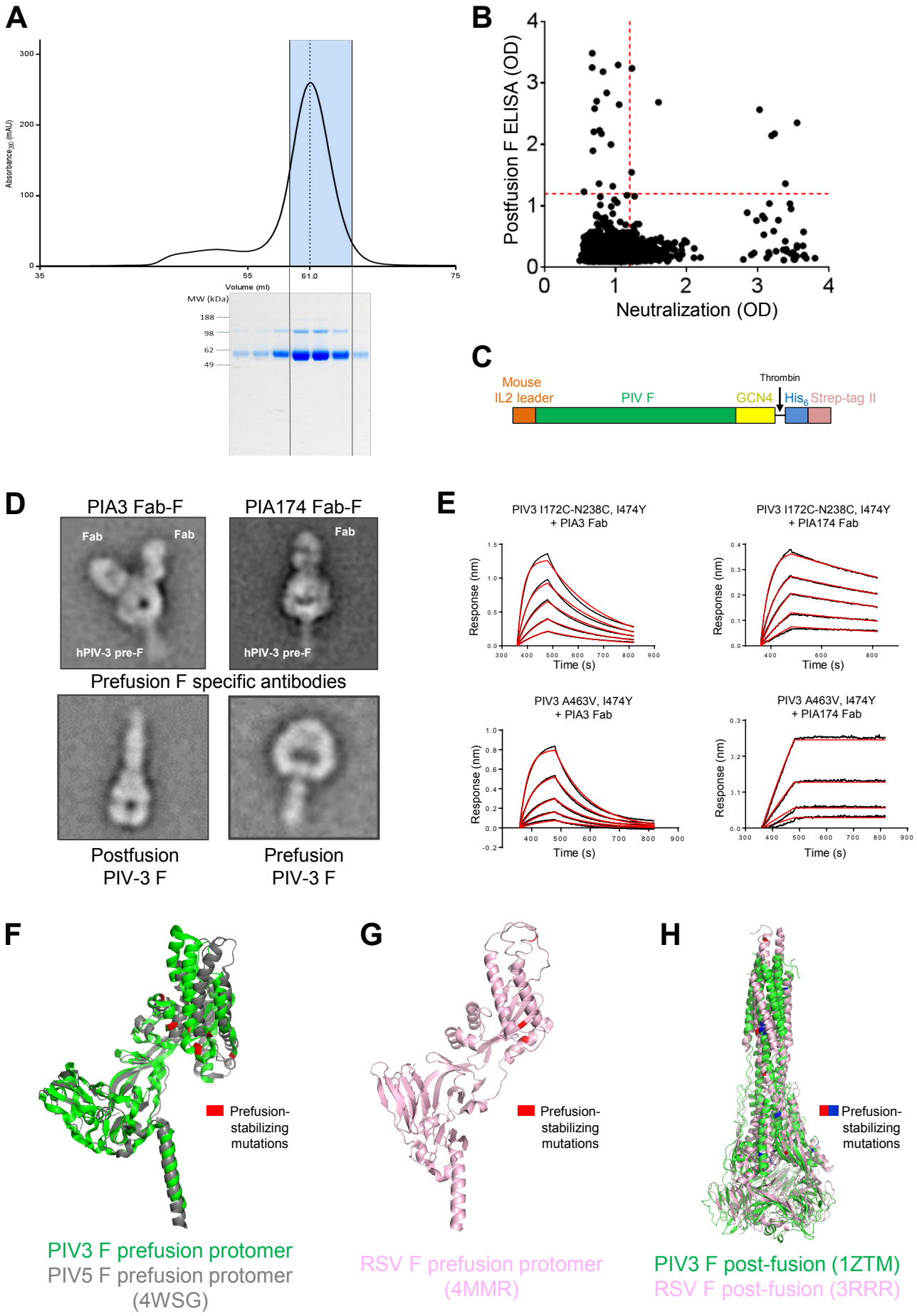
A
Absorbance280 (mAU)
Volume (ml)
MW (kDa)
188
98
62
49
B
Postfusion F ELISA (OD)
Neutralization (OD)
C
Mouse
IL2 leader
PIV F
GCN4
Thrombin
His6 Strep-tag II
D
PIA3 Fab-F
PIA174 Fab-F
Fab
hPIV-3 pre-F
Prefusion F specific antibodies
Postfusion
PIV-3 F
Prefusion
PIV-3 F
E
PIV3 I172C-N238C, I474Y
+ PIA3 Fab
PIV3 I172C-N238C, I474Y
+ PIA174 Fab
PIV3 A463V, I474Y
+ PIA3 Fab
PIV3 A463V, I474Y
+ PIA174 Fab
Response (nm)
Time (s)
F
Prefusion-
stabilizing
mutations
PIV3 F prefusion protomer
PIV5 F prefusion protomer
(4WSG)
G
Prefusion-
stabilizing
mutations
RSV F prefusion protomer
(4MMR)
H
Prefusion-
stabilizing
mutations
PIV3 F post-fusion (1ZTM)
RSV F post-fusion (3RRR)

Fig. S1. Isolation and characterization of prefusion or postfusion PIV3 F-specific monoclonal antibodies. (A) Superdex 200 gel filtration profile of postfusion PIV3 F and SDS-PAGE analysis. (B) Analysis of PIV3 neutralization and binding to postfusion F protein of cloned human B-cell supernatants, revealing potently neutralizing antibodies that did not bind recombinant postfusion F and antibodies of low potency that bind recombinant postfusion F, allowing identification of PIA56 and PIA75 (postfusion F specific) and PIA3 and PIA174 (prefusion F specific) antibodies. (C) Schematic showing the overall design and arrangement of the elements in the prefusion PIV F expression constructs. (D) Negative stain 2D averages of PIV3 F co-expressed with Fabs from PIA3 (top left), PIA174 (top right), without stabilizing mutations (lower left) and with prefusion-stabilizing mutations (lower right). (E) Representative octet interferometry profiles for binding of PIA3 or PIA174 Fabs to PIV3 prefusion-stabilized F variants (data in Fig. S2). (F) Comparison by superimposition of prefusion PIV5 F (4WSG) coordinates with prefusion PIV3 F cryo-EM protomer coordinates, highlighting PIV3 prefusion F-stabilizing mutations in red. (G) RSV prefusion F protomer (DS-Cav1) showing prefusion F-stabilizing mutations shown in red. (H) Despite low sequence homology between RSV and PIV3 F sequences (~35%), when comparing PIV3, and RSV postfusion coordinates the structures adopt similar postfusion conformations (PIV3 prefusion F-stabilizing mutations are shown in blue and RSV prefusion F-stabilizing mutations are shown in red).

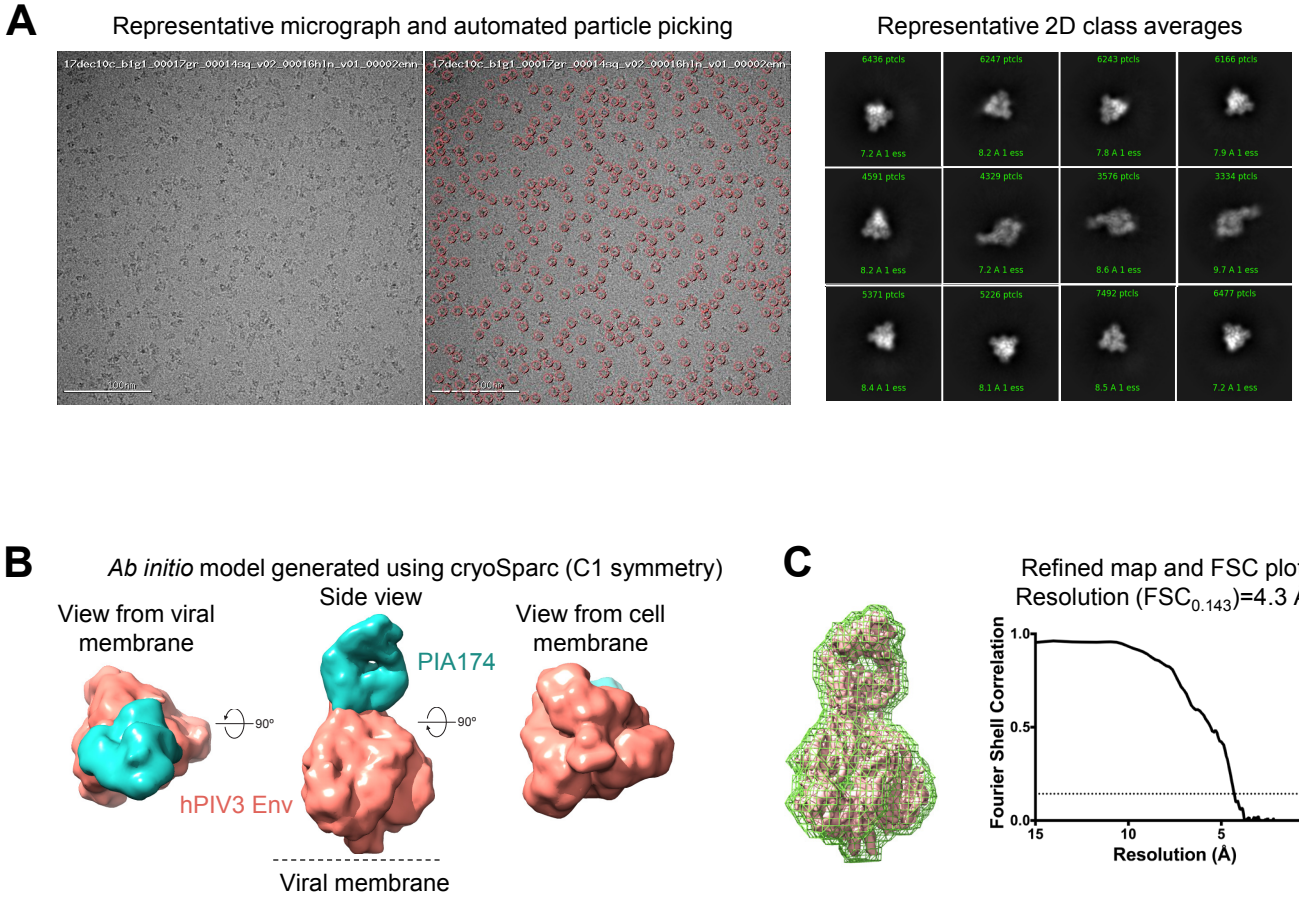

Fig. S2. Details of cryo-EM structure of PIV3 prefusion F Q162C-L168C, I213C-G230C, A463V, I474Y in complex with Fab PIA174. (A) Representative micrograph (left) with particles picked with DogPicker shown in red circles (middle). Representative 2D class averages (right). (B) *Ab initio* model generated using cryoSparc showing PIV3 in salmon and PIA174 Fab in cyan. (C) Refined map (left) used for post processing in RELION shown as green mesh. Fourier shell correlation plotted as a function of resolution with resolution reported according to the gold standard $FSC_{0.143}$ criterion ($FSC_{0.143}$ shown as dotted line) (right). (D) Representative electron density snapshots from different regions of the map shown as blue mesh with underlying fitted model shown in cartoon representation.

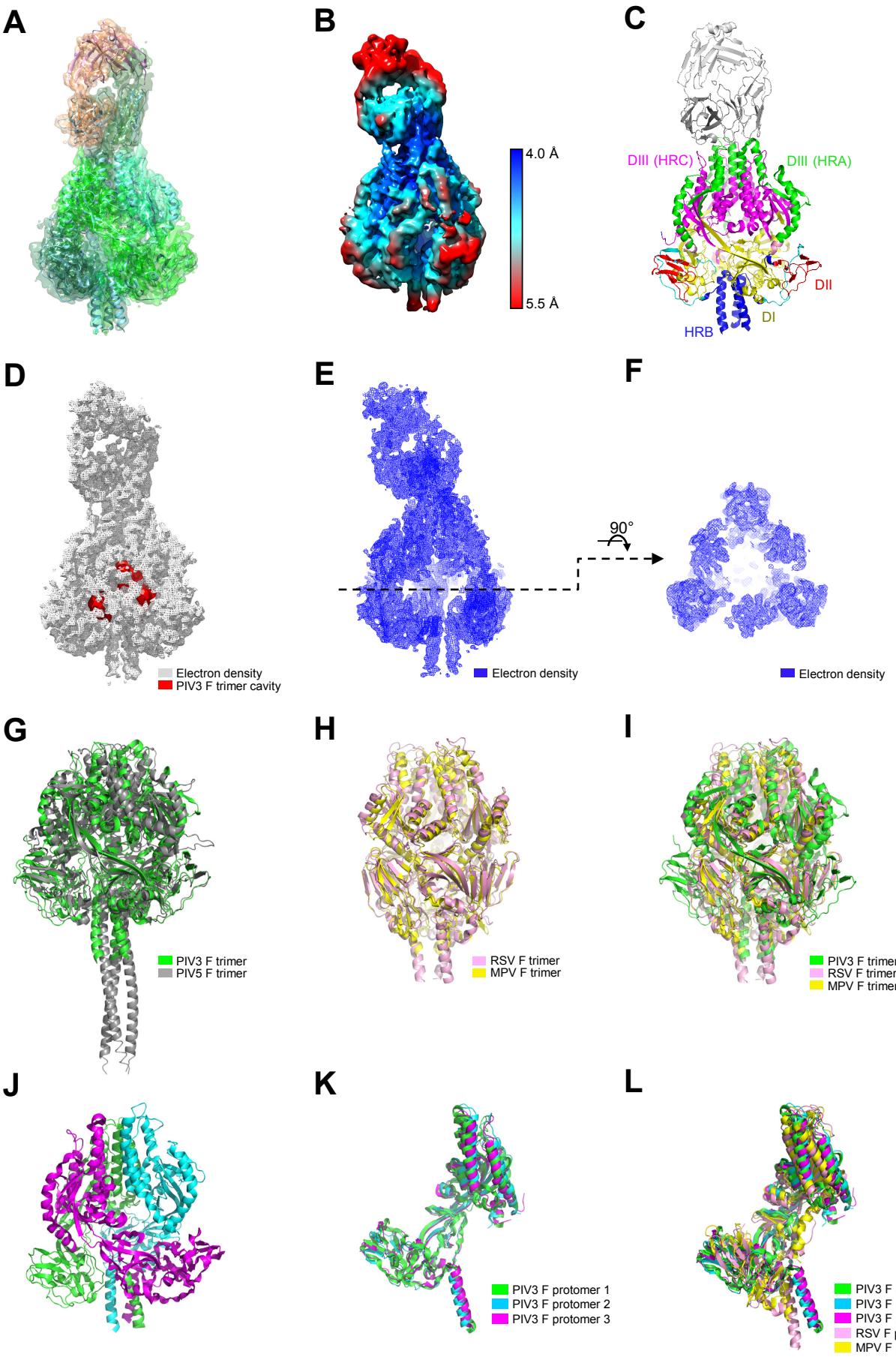
A
B
4.0 Å
5.5 Å
C
DIII (HRC)
DIII (HRA)
DII
DI
HRB
D
Electron density
PIV3 F trimer cavity
E
Electron density
90°
F
Electron density
G
PIV3 F trimer
PIV5 F trimer
H
RSV F trimer
MPV F trimer
I
PIV3 F trimer
RSV F trimer
MPV F trimer
J
K
PIV3 F protomer 1
PIV3 F protomer 2
PIV3 F protomer 3
L
PIV3 F protomer 1
PIV3 F protomer 2
PIV3 F protomer 3
RSV F protomer
MPV F protomer 3

Fig. S3. Structural analysis of prefusion-stabilized PIV3 F Q162C-L168C, I213C-G230C, A463V, I474Y in complex with PIA174 Fab and comparison with PIV5, RSV and MPV prefusion F glycoprotein structures. (A) Map segmented by chains, with underlying fitted model for the PIV3 F Q162C-L168C, I213C-G230C, A463V, I474Y-PIA174 Fab complex. (B) Local resolution distribution for the PIV3 F Q162C-L168C, I213C-G230C, A463V, I474Y-PIA174 Fab complex revealing the most ordered regions to be the prefusion PIV3 F trimer core area and the interface with PIA174 Fab. (C) PIV3 F trimer domain organization showing DI (yellow), DII (red), DIII HRA (green) and DIII HRC (magenta). (D) Prefusion PIV3 F central cavity and electron density map showing internal aqueous cavity in red. (E) Prefusion PIV3 F-PIA174 Fab map sectioned to show internal aqueous cavity. (F) 90° section of prefusion PIV3 F trimer electron density showing internal aqueous cavity. (G) Superimposition of prefusion PIV5 F trimer (4WSG) and prefusion PIV3 F trimer, contrasted to a superimposition of prefusion HRSV (4MMR) and HMPV (5WB0) shown in (H), where trimers adopt a more oblong overall shape, and the more rounded shape of the prefusion PIV3 F compared to HRSV and HMPV F structures shown in (I). The intertwining and asymmetric prefusion PIV3 F protomers are shown in (J) for trimer and (K) for superimposed individual protomers from the PIV3 F trimer. However the PIV3 protomers differ markedly from the prefusion HRSV and HMPV F in structures (L), yet retain a similar general domain organization.

Design	Oligomeric state	Elution volume (mL)†	Yield (mg/L)	Antibody K_D value (nM)						Physical stability (fractional PIA174 reactivity)						
				PIA3	PIA3	PIA3	PIA174	PIA174	PIA174	Temp (ºC)		pH		Freeze /Thaw	Osmolality (mM)	
				(1:3)	K_{on}	K_{off}	(1:1)	K_{on}	K_{off}	50	70	3.5	10		10	3000
PIV3 F GCN4	Trimer	16.07	0.2	74.4	1.18E+05	8.79E-03	<0.001	7.19E+04	<1.0E-07	0.9	0	0	0.4	0.8	0.5	0.6
PIV3 F GCN4, 172C-238C	Trimer	16.19	2.2	23.6	1.77E+05	4.19E-03	20.5	3.72E+04	7.62E-04	1.2	0	1.2	1.2	0.6	1.2	1.4
PIV3 F GCN4, A464V	Trimer	16.01	0.6	92.8	9.00E+04	8.35E-03	<0.001	1.73E+06	<1.0E-07	0.3	0.1	0.1	0	0.1	0.1	0.5
PIV3 F GCN4, A464V, I474Y	Trimer	16.18	1.6	29.8	2.48E+05	7.48E-03	<0.001	3.19E+05	<1.0E-07	0.9	0	0	0.4	0.9	0.6	0.6
PIV3 F GCN4, Y178W	Trimer	16.01	<0.1	N.B.	N/A	N/A	N.B.	N/A	N/A	N/A	N/A	N/A	N/A	N/A	N/A	N/A
PIV3 F GCN4, Y178W, A464V, I474Y	Trimer	15.51	0.2	N.B.	N/A	N/A	N.B.	N/A	N/A	N/A	N/A	N/A	N/A	N/A	N/A	N/A
PIV3 F GCN4, 172C-238C, Y178W	Trimer	16.23	0.5	43.2	2.08E+05	5.18E+03	33.9	7.34E+04	2.49E-03	1	0.1	1.2	0.7	0.8	0.7	1
PIV3 F GCN4, 172C-238C, I474Y	Trimer	16.48	3.2	31.7	1.55E+05	4.91E-03	9.75	9.78E+04	9.54E-04	0.8	0	1.3	0.8	0.6	0.8	0.6
PIV3 F GCN4, 172C-238C, A464V, I474Y	Trimer	16.34	2.9	29.8	1.51E+05	4.49E-03	10.6	9.10E+04	9.66E-04	1	0.3	1	0.7	1	0.9	0.5
PIV3 F postfusion	Trimer	15.74	2.6	N.B.	N/A	N/A	N.B.	N/A	N/A	N/A	N/A	N/A	N/A	N/A	N/A	N/A
PIV3 F GNC4 V170C-I242C, A463V, I474Y	Trimer	61.16	11.9	247.3	7.29E+04	1.80E-02	0.3	2.27E+05	8.20E-05	0.7	0.1	1.3	0.6	0	0.7	0.7
PIV3 F GNC4 I213C-G230C, A463V, I474Y	Trimer	6.144	15.2	269.1	3.51E+04	9.45E-03	0.2	3.22E+05	7.23E-05	1.0	0.1	1.4	0.6	0	0.7	1.5
PIV3 F GNC4 D216C-L221C, A463V, I474Y	Trimer	61.30	5.7	235.2	5.18E+04	1.22E-02	<0.001	1.55E+04	<1.0E-07	1.0	0.2	0.4	0.4	0	0.3	0.5
PIV3 F GNC4 Q162C-L168C, A463V, I474Y	Trimer	61.12	10.3	79.1	7.74E+04	6.12E-03	<0.001	1.35E+04	<1.0E-07	1.0	0.1	0.6	0.6	0.1	0.8	0.9
PIV3 F GNC4 G85C-Q222C, A463V, I474Y	Trimer	61.61	8.2	414.7	3.46E+04	1.44E-02	<0.001	1.22E+04	<1.0E-07	0.9	0.1	1.0	0.5	0	0.5	1.0
PIV3 F GNC4 I172C-N238C, I474Y	Trimer	61.92		29.8	1.55E+05	4.91E-03	10.6	9.10E+04	9.66E-04							
PIV3 F GNC4 Q162C-L168C, V170C-I242C, A463V, I474Y	Trimer	61.16	12.5	661.2	2.00E+04	1.32E-02	<0.001	6.51E+05	<1.0E-07	0.9	0.5	1.3	0.6	0	0.8	0.5
PIV3 F GNC4 Q162C-L168C, I213C-G230C, A463V, I474Y	Trimer	61.61	23	229.4	1.91E+04	4.38E-03	<0.001	1.08E+05	<1.0E-07	0.9	0.1	1.7	1.3	0	1.3	0.3
PIV3 F GNC4 Q162C-L168C/D216C-L221C, A463V, I474Y	Trimer	61.92	15.8	200.4	2.24E+04	4.49E-03	<0.001	1.04E+05	<1.0E-07	0.9	0.1	1.1	0.6	0	0.8	0.8
PIV3 F GNC4 Q162C-L168C/G85C-Q222C, A463V, I474Y	Trimer	61.54	10.2	186.5	2.13E+04	3.96E-03	<0.001	1.04E+05	<1.0E-07	0.9	0.1	1.0	0.6	0	0.6	0.8
PIV3 F GNC4 I213C-G230C/V170C-I242C, A463V, I474Y	Trimer	61.73	13.3	1058	2.74E+04	2.90E-02	<0.001	3.40E+04	<1.0E-07	0.9	0.1	1.0	0.6	0	0.6	0.4
PIV3 F GNC4 I213C-G230C/D216C-L221C, A463V, I474Y	Trimer	61.19	11.9	500	2.06E+04	1.03E-02	0.18	8.16E+04	1.50E-05	1.0	0.2	1.2	0.1	0	0.7	0.4
PIV3 F GNC4 I213C-G230C/G85C-Q222C, A463V, I474Y	Trimer	61.30	3.5	676.1	2.09E+04	1.41E-02	<0.001	4.44E+04	<1.0E-07	1.0	0.4	1.2	0.6	0	0.8	0.5

Fig. S4. Antigenic characteristics of engineered PIV3 F glycoprotein variants.

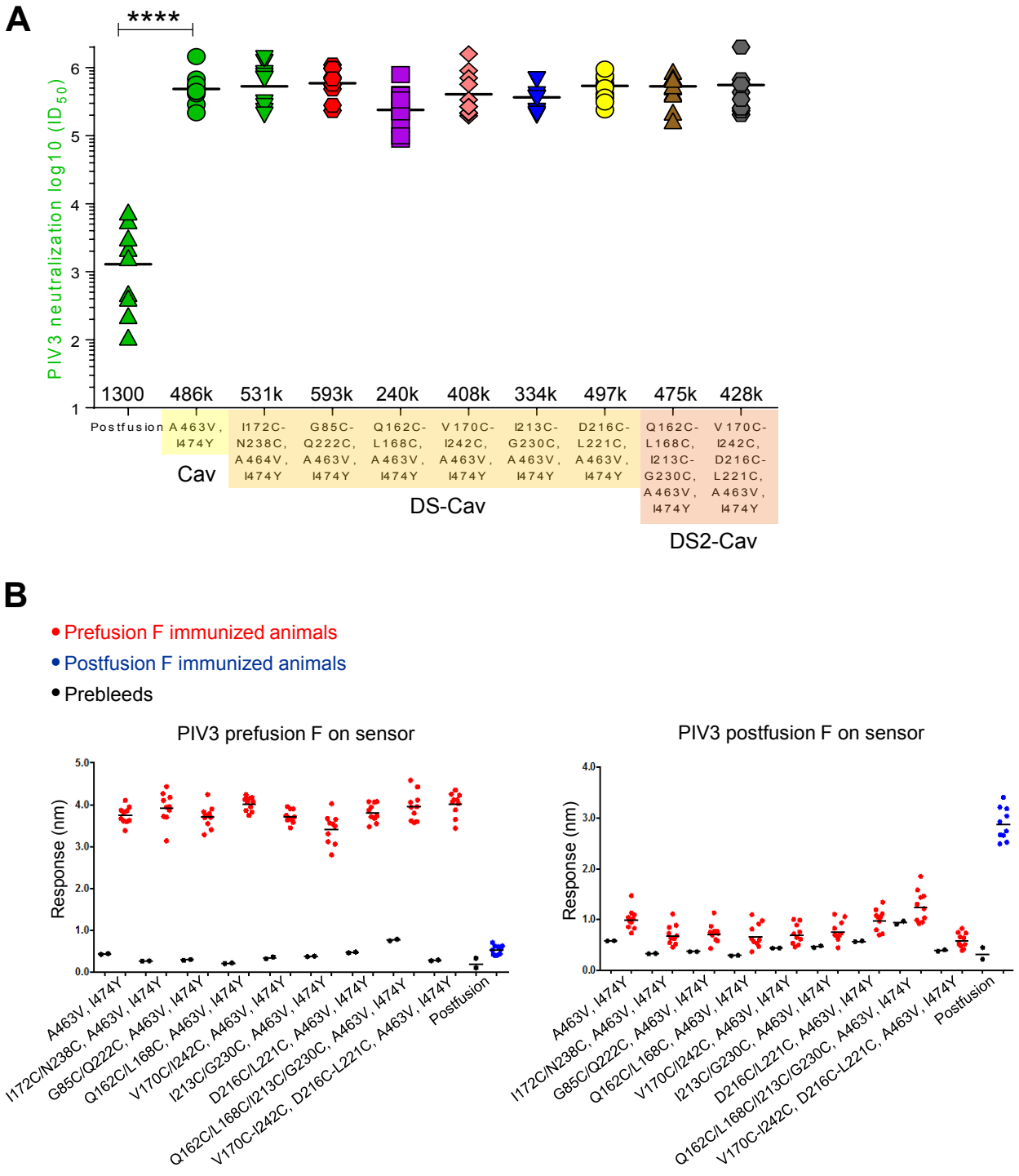

Fig. S5. Immunogenic analysis of engineered PIV3 F variants. (A) PIV3 serum neutralization for PIV3 immunogens immunized in CB6F1J mice, showing immunogens with cavity-filling mutations (Cav) in yellow, single disulfides with cavity-filling (DS-Cav) in orange and double disulfides with stabilized stem (DS2-Cav) in salmon. (B) Octet interferometry analyses of mouse sera using prefusion PIV3 F-coated sensors (left) and postfusion PIV3 F-coated sensors (right), demonstrating the serologic specificity of animal sera to their respective prefusion or postfusion F immunogens.

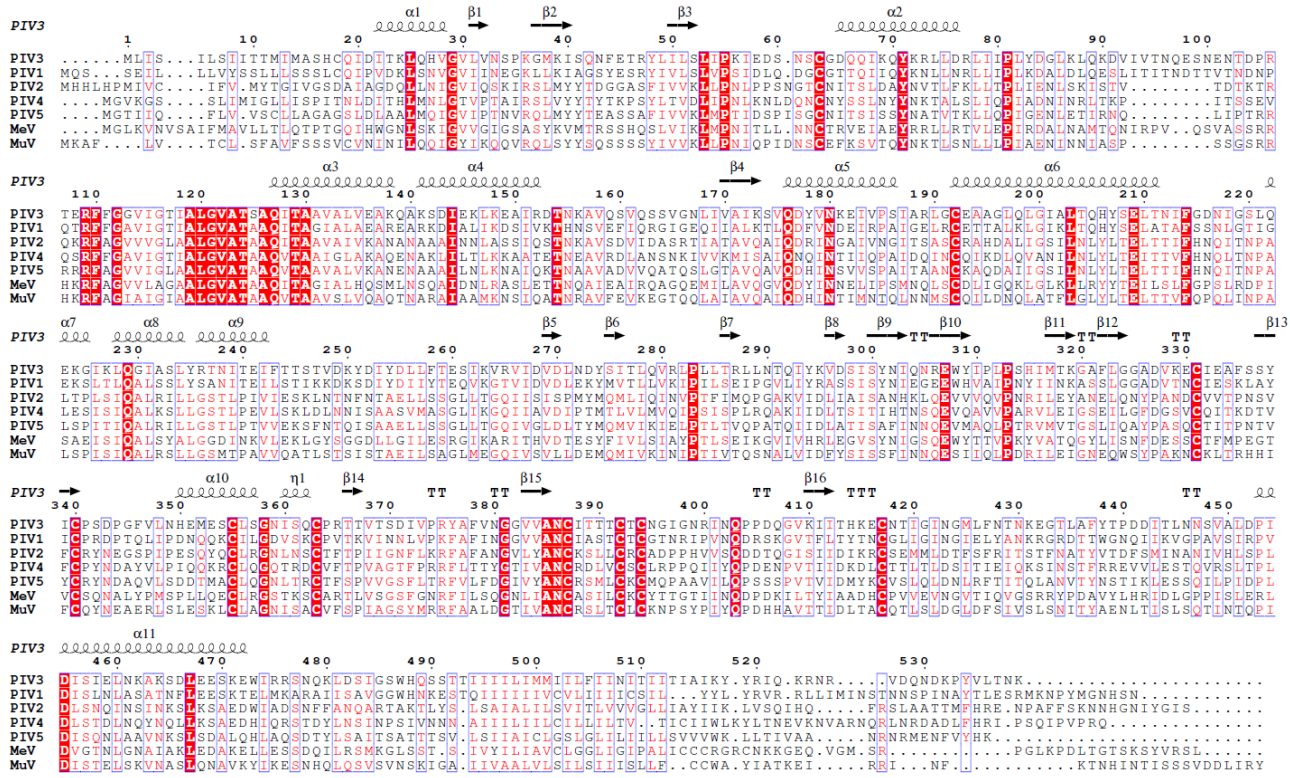

Fig. S6. Sequence comparison between PIV1-4, MeV and MuV F glycoproteins and analysis of PIV1, 2 and 4 F variants containing prefusion PIV3 F-stabilizing mutations. Sequence alignment for PIV1-4, MeV and MuV, showing the low homology between viral F genes within these human paramyxovirus family members that cause significant global disease burden.

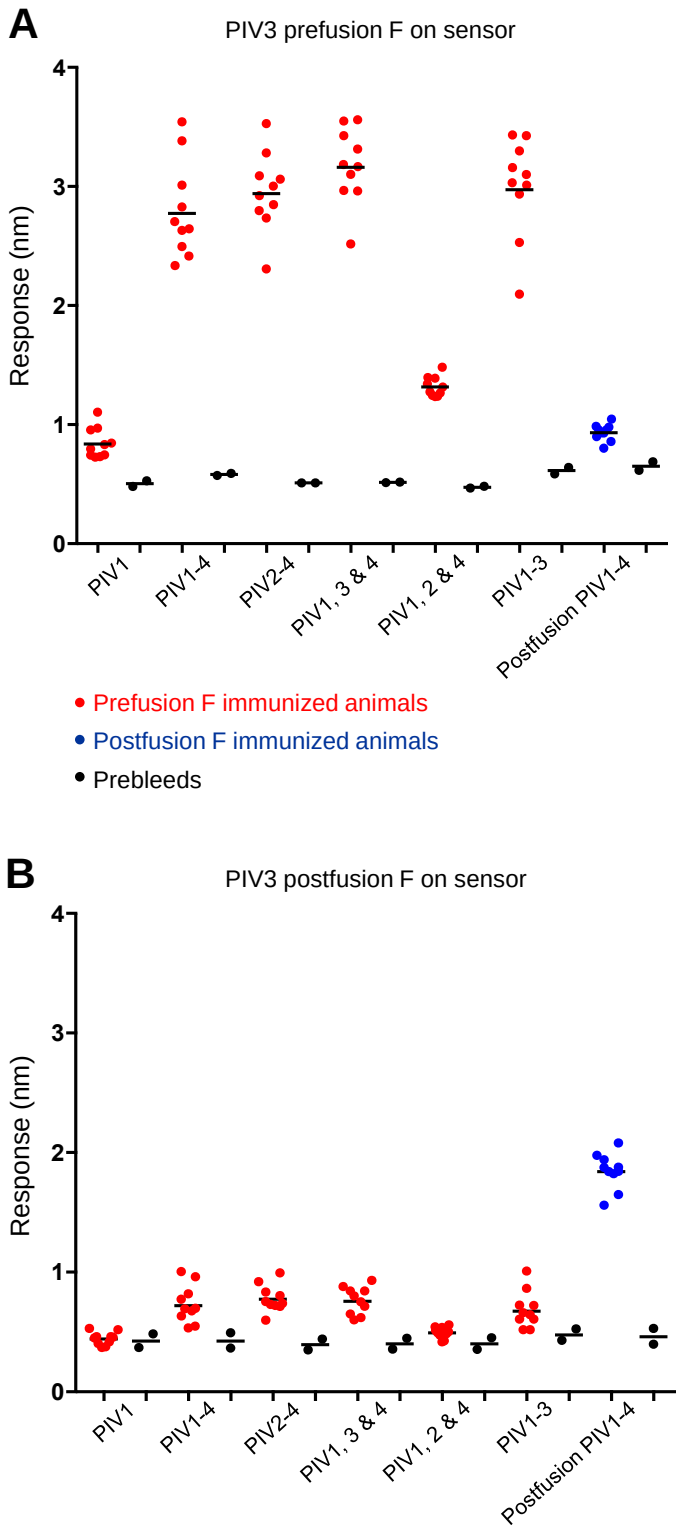

Fig. S7. Octet interferometry analysis of mouse sera from animals immunized with multivalent PIV1-4 immunogens. (A) PIV3 prefusion F-coated sensors or (B) PIV3 postfusion F-coated sensors were used to show prefusion and postfusion binding titers for monovalent, trivalent or quadrivalent immunogen groups. High-titer PIV3 prefusion F antibodies were elicited from all immunogens containing PIV3 prefusion F while omission of the PIV3 prefusion F component resulted in almost complete loss of immune recognition of PIV3 prefusion F, indicating a high serological specificity to the individual PIV prefusion F components.

Table S1. Antigenic characteristics of engineered PIV3 F glycoprotein variants.

Mechanism of stabilization	PIV3 F variant*	ELISA binding† upon expression				
		PIA3	PIA56	PIA75	PIA174	α-StrepTagII
C-terminal trimerization domain	Postfusion-Fd	0.18	0.19	0.06	0.14	0.72
	PIV3NO-GCN4	1.51	0.14	0.19	1.14	0.29
Helix-disrupting	A140P	0.35	0.20	0.05	0.12	0.25
	K141P	0.27	0.18	0.05	0.10	0.29
	S142P	2.70	0.70	0.21	1.31	0.35
	N155P	0.45	0.55	0.19	1.14	0.32
	A157P	3.42	1.32	0.28	2.55	0.53
	R189P	0.22	0.11	0.06	0.10	0.29
	L190P	0.06	0.10	0.06	0.10	0.29
	G191P	0.13	0.11	0.06	0.14	0.25
	E193P	1.17	0.15	0.06	0.22	0.24
	A194P	0.86	0.18	0.06	0.16	0.29
	A195P	0.27	0.13	0.06	0.10	0.30
	G196P	0.21	0.09	0.06	0.17	0.33
Disulfides	Y48C/I169C	0.17	0.09	0.05	0.10	0.24
	I50C/A171C	0.06	0.10	0.06	0.09	0.26
	S52C/K173C	0.16	0.11	0.05	0.17	0.26
	S60C/I187C	0.83	0.14	0.19	0.21	0.27
	N61C/I187C	1.18	0.13	0.12	0.38	0.27
	A139C/V268C	0.27	0.08	0.05	0.09	0.26
	A139C/D270C	0.06	0.09	0.06	0.10	0.22
	K140C/I269C	0.58	0.45	0.06	0.14	0.23
	K140C/D270C	0.06	0.09	0.05	0.11	0.22
	K141C/D258C	0.21	0.10	0.05	0.10	0.21
	K141C/D268C	0.22	0.10	0.05	0.10	0.16
	K143C/I269C	0.08	0.09	0.06	0.11	0.30
	K143C/D270C	0.09	0.09	0.06	0.15	0.26
	K143C/V271C	0.17	0.08	0.05	0.11	0.24
	I146C/V271C	0.14	0.10	0.05	0.10	0.24
	I146C/D272C	0.19	0.09	0.05	0.10	0.20
	E147C/D272C	0.25	0.11	0.05	0.10	0.25
	L149C/L273C	0.20	0.15	0.09	0.12	0.26
	L149C/N274C	0.06	0.13	0.06	0.10	0.26
	L149C/D275C	0.07	0.13	0.05	0.11	0.29
	I172C/N238C	3.12	0.51	0.11	2.56	1.02
	K181C/Q198C	0.06	0.10	0.05	0.10	0.29
	E182C/Q198C	0.10	0.10	0.06	0.10	0.16
	R365C/S448C	0.22	0.08	0.05	0.10	0.13
Disulfide + cavity filling	Y48C/I169C/V170L/I187F	0.13	0.07	0.05	0.10	0.33
	Y48C/I169C/D177C/S201C	0.06	0.09	0.06	0.09	0.56
	Y48C/I169C/Y178W	0.06	0.09	0.06	0.14	0.31
	Y48C/I169C/I57V/I183F/L199V	0.22	0.11	0.08	0.10	0.50
	S52C/K173C/V170L/I187F	0.18	0.08	0.06	0.10	0.30
	S52C/K173C/Y178W	0.19	0.11	0.05	0.17	0.28
	S52C/K173C/Q205W/R365C/S448C/D452W	0.24	0.08	0.06	0.09	0.14
	S52C/K173C/Q205W/D452W	0.06	0.08	0.06	0.10	0.23
	G85C/Q222C/A463V/I474Y	2.29	0.80	0.11	2.64	1.60
	K141C/D258C/V170L/I187F	0.25	0.09	0.07	0.10	0.36

* All mutations were assessed on wild type PIV F with a C-terminal his_6-StrepTagII tandem purification tag.
† Optical density at 450 nm assessed in a 96-well format as described in Methods.

Table S1 (continued). Antigenic characteristics of engineered PIV3 F glycoprotein variants.

Mechanism of stabilization	PIV3 F variant*	ELISA binding† upon expression				
		PIA3	PIA56	PIA75	PIA174	α-StrepTagII
Disulfide + cavity filling	K141C/D258C/Y178W	0.10	0.10	0.05	0.13	0.28
	K141C/D258C/Q205W	0.09	0.09	0.06	0.10	0.26
	Q162C/L168C/A463V/I474Y	2.32	1.05	0.14	2.64	1.81
	V170C/I242C/A463V/I474Y	2.31	1.33	0.12	2.66	1.41
	I172C/N238C/E193P	2.96	0.78	0.10	2.61	1.30
	I172C/N238C/A464V	2.95	0.42	0.15	2.55	0.75
	I172C/N238C/I474Y	3.02	1.49	0.12	2.76	1.13
	I172C/N238C/A188P	3.08	0.69	0.07	0.17	0.55
	I172C/N238C/V170L/I187F	0.87	0.09	0.06	0.13	0.39
	I172C/N238C/V170L/I187F	0.76	0.10	0.06	0.12	0.38
	I172C/N238C/Y178W	3.05	0.51	0.06	0.85	0.36
	I172C/N238C/A188P/Q205W	2.76	0.51	0.08	0.12	0.87
	I172C/N238C/Q205W/D452W	2.59	1.86	0.13	1.91	0.57
	I172C/N238C/D452W	3.07	1.30	0.23	2.69	1.07
	I213C_G230C_A463V_I474Y	2.47	1.12	0.17	2.84	1.63
	K224C_R265C_A463V_I474Y	2.41	1.38	0.15	2.59	1.63
	R365C/S448C/Q205W/D452W	0.07	0.09	0.06	0.14	0.14
Cavity filling	Q127W	0.19	0.13	0.06	0.15	0.20
	A131L	0.24	0.13	0.05	0.09	0.19
	E145L	2.03	0.28	0.21	0.34	0.19
	T154D	0.17	0.93	0.27	1.90	0.54
	T154R	0.23	0.15	0.11	0.14	0.24
	V165T	3.38	1.05	0.27	2.13	0.48
	V165R	3.25	0.99	0.17	2.21	0.55
	V170I	1.91	0.23	0.21	0.31	0.22
	K173L	0.09	0.16	0.05	0.09	0.31
	V175I	2.77	0.28	0.20	0.53	0.23
	V179L	0.25	0.14	0.06	0.10	0.21
	I187F	0.26	0.10	0.05	0.09	0.23
	Q205W	0.09	0.09	0.06	0.10	0.23
	D452W	0.39	0.18	0.06	0.11	0.17
	D452R	1.75	0.31	0.23	0.30	0.28
	A463I	2.43	0.56	0.25	0.38	0.13
	A464I	1.83	0.43	0.15	0.39	0.13
	A464V	2.30	0.24	0.22	0.54	0.12
	S470L	2.22	0.28	0.22	0.38	0.15
	S470I	1.58	0.19	0.28	0.32	0.11
	S470V	2.29	0.23	0.26	0.42	0.13
	I474Y	2.76	1.21	0.18	2.42	1.16
	S477L	1.65	0.21	0.22	0.30	0.16
	S477I	2.14	0.20	0.24	0.34	0.17
	S477V	2.51	0.24	0.26	0.49	0.30
	L49F/V170I/I172V/I242L	0.34	0.14	0.09	0.12	0.26
	L49F/V170L/I172G/I242Y	0.29	0.10	0.08	0.09	0.35
	L49F/V170I/I172V/I242L/S52F/I151L/A171G	0.25	0.11	0.07	0.20	0.32
	I50M/E145F/D268G/T277L	0.05	0.09	0.05	0.10	0.24
	S52M/I151L	3.06	0.74	0.24	0.95	0.19
	S52F/I151L/A171G	0.22	0.27	0.26	0.65	0.23

* All mutations were assessed on wild type PIV F with a C-terminal his_6-StrepTagII tandem purification tag.
† Optical density at 450 nm assessed in a 96-well format as described in Methods.

Table S1 (continued). Antigenic characteristics of engineered PIV3 F glycoprotein variants.

Mechanism of stabilization	PIV3 F variant*	ELISA binding† upon expression				
		PIA3	PIA56	PIA75	PIA174	α-StrepTagII
Cavity filling	S52G/I151L/A171F	0.26	0.12	0.05	0.11	0.25
	D59F/Q127W/S220L/E223F	0.06	0.14	0.05	0.09	0.12
	D59F/Q127W/S220L/E223F/V170I/I172V/I242F	2.31	0.64	0.22	0.48	0.20
	D59F/Q127W/S220L/E223F/I50M/E145F/D268G/T277L	0.24	0.11	0.07	0.10	0.19
	D59Y/N61M/D65F/I187F	0.10	0.09	0.06	0.13	0.21
	D59A/N61V/D65F/I187F	0.30	0.10	0.05	0.11	0.20
	D59A/N61V/D65F/I187F/S174G/V175I/H206F	0.21	0.10	0.06	0.11	0.18
	D59Y/N61M/D65F/I187F/Q89F/V94F/E223F	0.06	0.08	0.09	0.10	0.21
	Q89F/V94I/A131F/E223L	0.19	0.20	0.07	0.20	0.28
	Q89F/V94I/A131F/E223F	0.10	0.11	0.06	0.17	0.28
	Q89F/V94F/E223F	1.28	0.41	0.11	1.14	0.55
	Q127W/A131L	0.05	0.08	0.05	0.09	0.16
	Q127W/A131L/V170I/V175I/V179L	0.15	0.09	0.06	0.10	0.14
	Q127W/A131L/K173L/E145L	0.23	0.10	0.06	0.10	0.20
	A130F/E223M/R265W/R281M	0.45	0.20	0.09	0.32	0.30
	A130F/E223L/R265W/R281I	0.20	0.17	0.06	0.11	0.27
	A130F/E223L/R265W/R281I/S52G/I151L/A171F	0.26	0.15	0.08	0.10	0.32
	E145L/D268L/T277L	0.24	0.09	0.06	0.09	0.19
	E145M/D268A/T277L	0.07	0.09	0.06	0.14	0.24
	E145L/D268L/T277L/Q89F/V94I/A131F/E223L	0.26	0.08	0.08	0.10	0.19
	V170I/I172V/I242F	3.07	0.54	0.26	0.74	0.26
	V170I/V175I/V179L	0.06	0.13	0.05	0.09	0.17
	V170I/V175I/V179L/K173L/E145L	0.08	0.12	0.06	0.16	0.34
	K173L/E145L	0.19	0.21	0.05	0.09	0.22
	S174F/V175I/H206M	0.24	0.12	0.06	0.10	0.19
	S174G/V175I/H206F	0.33	0.18	0.07	0.11	0.17
	S174F/H206L	0.11	0.11	0.10	0.12	0.29
	S174F/H206L/A130F/E223M/R265W/R281M	0.08	0.14	0.06	0.10	0.30
	I187F/Q127W/A131L	0.26	0.08	0.06	0.09	0.12
	I187F/V170I/V175I/V179L	0.16	0.08	0.06	0.13	0.23
	I187F/V170I/V175I/V179L/Q127W/A131L/K173L/E145L	0.11	0.09	0.06	0.13	0.24
	I187F/K173L/E145L	0.14	0.11	0.05	0.10	0.27
	E193P/A464V	0.90	0.13	0.07	0.28	0.14
	I474Y/A464V	2.70	0.27	0.25	2.39	0.44
Cavity filling + helix disrupting	I474Y	2.72	1.07	0.25	2.47	0.74
	I474Y/E193P	1.63	0.37	0.08	0.57	0.55
	V170L/I187F/E193P	0.11	0.08	0.08	0.09	0.24

* All mutations were assessed on wild type hPIV F with a C-terminal his_6-StrepTag II tandem purification tag.
† Optical density at 450 nm assessed in a 96-well format as described in Methods.

Table S2. Cryo-EM data collection and refinement statistics.

	PIV3 Q162C-L168C, I213C-G230C, A463V, I474Y F – PIA 174 Fab
Data Collection	
Microscope	FEI Titan Krios
Voltage (kV)	300
Electron dose ($e^-/Å^2$)	56.3
Detector	Gatan K2 Summit
Pixel Size (Å)	1.1
Defocus Range (μm)	-1- -1.7
Magnification	105000
Reconstruction	
Software	cryoSparc
Particles	97177
Symmetry	C1
Box size (pix)	320
Resolution (Å) ($FSC_{0.143}$)$	4.3
Refinement (Phenix)#	
Protein residues	1479
Chimera CC	0.87
Resolution ($FSC_{0.5}$)	4.4
EMRinger Score	0.95
R.M.S. deviations	
Bond lengths (Å)	0.005
Bond angles (°)	0.913
Validation	
Molprobity score	1.88
Clash score	7.52
Favored rotamers (%)	95.6
Ramachandran	
Favored regions (%)	88.2
Allowed regions (%)	11.66
Disallowed regions (%)	0.14

$ Resolutions are reported according to the $FSC_{0.143}$ gold-standard criterion.
# Statistics are reported for the protein residues within the complex excluding the antibody constant domains.